IEEE Access
Multidisciplinary | Rapid Review | Open Access Journal

SPECIAL SECTION ON DATA ANALYTICS AND ARTIFICIAL INTELLIGENCE FOR PROGNOSTICS AND HEALTH MANAGEMENT (PHM) USING DISPARATE DATA STREAMS

Received November 7, 2019, accepted November 26, 2019, date of publication December 4, 2019,
date of current version December 23, 2019.

Digital Object Identifier 10.1109/ACCESS.2019.2957599

Load-Dependent Rotating Performance of Motorized Spindles: Measurement and Evaluation Using Multi-Zones Error Map

WEIZHENG CHEN, ZHAOJUN YANG, CHUANHAI CHEN, AND WEI LUO
School of Mechanical and Aerospace Engineering, Jilin University, Changchun 130025, China
Key Laboratory of CNC Equipment Reliability, Ministry of Education, Jilin University, Changchun 130025, China

Corresponding author: Chuanhai Chen (cchchina@foxmail.com)

This work was supported in part by the National Science and Technology Major Project under Grant 2018ZX04039001, in part by the National Natural Science Foundation under Grant 51975249 and Grant 51675227, in part by the Jilin Province Science and Technology Development Funds under Grant 20180201007GX and Grant 20190302017GX, and in part by the Fundamental Research Funds for the Central Universities.

ABSTRACT The rotating performance of motorized spindles is critical to the dimensional accuracy and surface quality of the parts to be machined. This paper proposes a novel measurement strategy and an evaluation method of spindle's rotating performance, considering the loads imposed on the spindle. To be specific, cutting loads are simplified as a unified function to guide the load simulation, and the load-induced error is eliminated using a position adjustment procedure. In a certain speed-load combination, the spindle's rotating performance under the unified load function is measured using a data envelope method. To extend the assessment to all typical work conditions, an evaluation scheme for different speed and load combinations is proposed based on a visual ideal of Multi-Zones Error Map (MZE Map). The necessity of considering the load-dependent rotating performance is demonstrated via several tests conducted on proposed load simulation platform. Besides, the procedures for developing the MZE Map are performed, and the results express an overview relationship between rotating performance and different speed-load conditions. The proposed method provides a new approach to evaluate the rotating performance considering the actual load conditions. This load-dependent oriented evaluating strategy contributes to a more precise health evaluation and management method for motorized spindles in actual machining process.

INDEX TERMS Rotating machines, load modeling, performance evaluation, prognostics and health management.

I. INTRODUCTION

Motorized spindles are the critical component in advanced CNC machine tools [1], the rotating performance of which determines the machining quality of work piece. Researches indicate that the radial rotating error of the motorized spindle critically affects the machining performance, not only because of its relatively large value but also its influence on cutting dynamic [2], [3]. Thus, the quantitative analysis of spindle's radial rotating motions is essential for performance evaluation and health management [4], [5].

The rotating orbit reveals the spindle's shaft center position concerning the mechanical performance of the spindle. Although the traditional radial run out test is the most direct method of quantifying radial rotating error, it only indicates the rotating performance in non-rotating conditions [6]. Since the radial motions of spindle vary significantly with different rotation speeds, as described in [2] and [7], the speed-dependent evaluation for rotating spindles has been widely recognized as a popular evaluation method [8]. Anandan and Ozdoganlar [9] systematically concluded the uncertainty factor and magnitude in the speed-dependent radial motion test and suggested some approaches to reduce detection error. Nahata *et al.* [10] established a radial throw measurement method and predicting model when a spindle installed an actual cutting tool, the result of which is closer than the standard test bar.

However, the rotating motions are relevant not only with the rotating speed but also composite loads in the actual machining process. Varying loads and speed modulate both

The associate editor coordinating the review of this manuscript and approving it for publication was Qiang Miao.

the amplitude and frequency in displacement signals of rotating orbit [11]. Thus, the rotating orbit is non-stationary with time-varying spectrum elements. The traditional static test or stationary condition evaluation of the motorized spindle may not truly express the performance under these varying operation conditions. In recent years, Bediz *et al.* [12] and Ritou *et al.* [13] testified the dynamic response of spindles under different loads and rotating speed. However, the modal tests emphasize the identification of modal parameters, rather than the rotating performance, leading to the distinction in test signals and load pattern from the actual cutting loads. Some researches discussed the generality of the fault diagnosis method for different speed and load conditions [14], but they mainly focused on the classification problem. In [15], the author applied actual machining test to testify the performance of the CNC machine, yet, it is difficult to isolate the performance of the spindle itself. Although previous studies provide a foundation for evaluating the radial error motions of motorized spindles, a comprehensive and experimentally validated approach to determine the rotating performance considering both rotation speed and load conditions has yet to be completed.

Challenges arise in the evaluation of the rotating performance that considers different load conditions: Firstly, the loads are too complicated to control and apply to the motorized spindle. Secondly, the actual loads in the machining process are diverse and hard to be reproduced by the existing load simulating system; researchers are obliged to carry out the loading tests for some individual types of loads, for example, radial force in [16]. Thirdly, it is hard to describe the spindle's rotating orbit under the dynamic loads with conventional methods due to the complexity of the orbit shape. Besides, the precision of the measurement system needs further analysis to alleviate load-induced error factors. Fourthly, since there are too many factors in dynamic loads, it is difficult to establish and display the complete relationship among all variables and rotating performance. For instance, the Stability Lobe Diagram (SLD) improves the visualization of test results with a stable zone in the diagram [17], [18] but it fails to present all performance information during typical machining process. Thus, a practical and visual expression for load-dependent performance needs to be customized. The colorful status map in [19] plays a visual role in distinguishing different health conditions for locating unwanted parts.

In order to solve the above challenges, a simplified load function and a corresponding load simulation test platform are presented in this paper. The difficulty in describing dynamic rotating orbit is overcome through an enveloping circle after eliminating the detection error during the measurement of rotating orbit. Furthermore, a Multi-Zones Error Map is designed, which serves as a visual tool for presenting rotating performance under different speed and load conditions. In contrast with the conventional evaluation approach, the proposed method discovers more performance-related information, assisting the health evaluation of motorized spindles in a more precise way.

II. MEASUREMENT OF LOAD-DEPENDENT MOTIONS

The rotating performance of motorized spindles under load conditions is difficult to be measured due to the lack of unified load function for guiding load-dependent tests, the complexity of the load simulation platform, and the difficulty of isolating measurement error introduced by loads. In this section, these three challenges are discussed to establish a precise strategy for measuring the load-dependent rotating orbit of motorized spindles.

A. UNIFIED LOAD FUNCTION

A practical and applicable load function guides the pattern and in the load-related test. Kaymakci *et al.* [20] proposed a unified load model for metal cutting operations based on a transferred load function, which simulates any load conditions of the motorized spindle is established in this section.

In all mental cutting processes, the normal force F_v and friction force on the rake face F_u are the critical loads that relevant to tool geometry, material character, and machining parameters [21]. And F_v and F_u are regarded as constants for simplification when machining parameters are determined.

There are two steps to transfer the cutting force from rake face to the motorized spindle. Firstly, Matrix T_{RU} is used to transfer loads from the rake face frame (UV) to Radial-Tangential-Axial (RTA) coordinates of the tool body frame (TB), and T_{RU} depends merely on the tool's geometry. Secondly, T_{OR} is the transfer matrix from the tool body frame (TB) to the spindle frame (XYZ), which depends on the processing type as Eq. 1. Each insert is placed on a rotating or a stationary tool body by applying the orientation angle ($\psi_{i,j}$) of the insert [20].

$$T_{OR} = \begin{bmatrix} sin\psi_j & -cos\psi_j & 0 \\ cos\psi_j & sin\psi_j & 0 \\ 0 & 0 & 1 \end{bmatrix} \tag{1}$$

a) Milling: $\psi_j = \varphi_0 + \sum_{j=1}^{N} \varphi_{pj} - \theta_i + \omega t$
b) Drilling-indexed boring: $\psi_j = \varphi_0 + \sum_{j=1}^{N} \varphi_{pj} + \omega t$
c) Turning and single point boring: $\psi_j = -\frac{\pi}{2}$

where φ_0 is the reference insert's angular position, φ_{pj} is the pitch angle of segment i in insert j on the circumference of the cutter. θ_i is the lag angle caused by the helical edge. The total forces can be evaluated by accumulating the differential forces contributed by all teeth (N) and edge segments (K), as shown in Eq.2. The cutting torque is calculated by the product of tangential force and insert's distance to the rotating center (D_{ci}).

$$\begin{cases} dF_i = \begin{Bmatrix} dF_{Xj} \\ dF_{Yj} \\ dF_{Zj} \end{Bmatrix}_i = T_{OR} \cdot T_{RU} \cdot \begin{Bmatrix} dF_{uj} \\ dF_{vj} \end{Bmatrix}_i \\ dM_i = N \cdot \begin{bmatrix} 0 & 0 & 0 \\ 0 & 1 & 0 \\ 0 & 0 & 0 \end{bmatrix} \cdot T_{RU} \cdot \begin{Bmatrix} dF_u \\ dF_v \end{Bmatrix}_i \cdot D_{ci} \end{cases} \tag{2}$$

Based on Eq. 2, the overall loads imposed on a spindle is consist of radial force F_r (consist of F_x and F_y), axial force

$F_a(F_z)$, and torque M. In this paper, the simplified loads $\boldsymbol{L_i}$ is defined to represent the loads that applied to a motorized spindle as Eq. 3, which serves as the guidance for the load-dependent test. The type of machining process is noted with index label i.

$$\boldsymbol{L_i} = \{F_r, F_a, M\}, \quad i = 1, 2 \cdots I \tag{3}$$

In the milling process, the radial force F_r is regarded as the dominant loads due to its direct influence on the radial motions [22]. According to Eq. 1, the radial force can be simplified as a sinusoidal period function, which is caused by the approximate circle motions of dynamic cutting thickness [23]. According to Eq. 2, the axial force (F_z) is not relevant to the rotating angle. Thus it can be regarded as a constant value. In the drilling and boring process, the axial force is defined as the dominant loads because of its relatively high amplitude [24]–[26]. Due to the symmetry of the cutting force, the fundamental value of the radial force in drilling and boring is zero in most cases. The cutting torque can be simulated as constant when cutting parameters are determined (refer to Eq. 2). The process damping and other random factors in the cutting loads can be assembled into a noise function $\sigma(t)$.

To sum up, the simplified load function $\boldsymbol{L_i}$ for the mill, drilling, and boring process can be expressed based on both mathematics and experiment.

$$\boldsymbol{L_i} = \begin{Bmatrix} F_r \\ F_a \\ M \end{Bmatrix} = A \begin{Bmatrix} k_1 \\ k_2 \\ k_3 \end{Bmatrix} + \varepsilon \begin{Bmatrix} sin(30N\pi nt) \\ 0 \\ 0 \end{Bmatrix} + \sigma(t) \begin{Bmatrix} p_1 \\ p_2 \\ p_3 \end{Bmatrix} \tag{4}$$

The unified load function consists of a static component, a dynamic component, and a random component. In Eq. 4, A is the dominant value of the static component, ε is the amplitude of the dynamic component, n is the rotating speed. k_1, k_2, and k_3 are loads transferred factors according to the type of machining process, and they can be calibrated mechanistically from cutting tests [27]. p_1, p_2 and p_3 are the noise factors of different loads, which depends on the uncertainty level. In less precise situations, the noise factors can be set as zero for simplification. Some parameters in Eq. 4 alters with machining type:

a) Milling: $i = 1, k_1 = 1$.
b) Drilling and indexed boring:$i = 2, k_1 = 0, k_2 = 1$.
c) Turning and single point boring: $i = 3, k_2 = 1, \varepsilon = 0$.

B. LOAD-DEPENDENT TEST FRAMEWORK

In order to impose $\boldsymbol{L_i}$ on a motorized spindle precisely and regularly, a schematic diagram is proposed based on the design scheme in Fig. 1. A loading system exerts F_r, F_a, M simultaneously on the output end of the motorized spindle via a test tool. The loading device imposes F_r and F_a on a force converter, while the torque generated by dynamometer is applied to the test tool with a torque converter. A pair of displacement sensors is installed at the output of the motorized spindle to acquire its radial rotating orbit. As such,

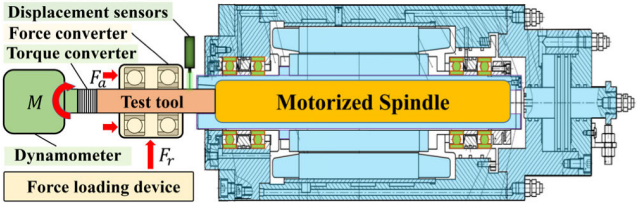

FIGURE 1. Schematics of the load-dependent precision test.

the rotating orbit of the motorized spindle under any speed and load combination can be simulated.

C. DETECTION ERROR IN LOAD-DEPENDENT TEST

In the ideal situation, the cross line of displacement sensors (detection coordinates) should coincide with the spindle's shaft center. However, it is impossible to realize in a dynamic loading situation since the shaft center is shifting by both rotating error and load-induced error. The detection error in load-dependent test arises from the following sources: (1) installation error of the displacement sensors from the ideal position, (2) relative deviation between spindle center and displacement sensors which caused by rotating error and deformation of spindle due to loads, (3) vibration and (4) the accuracy of loading system. In this section, the error source caused by the first two factors is analyzed and alleviated through an adjustment approach.

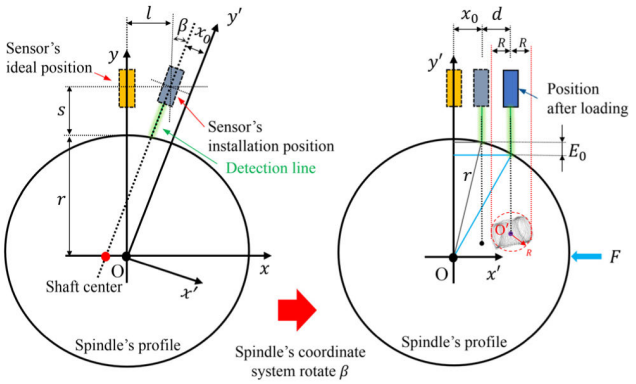

FIGURE 2. Geometric of deviation error of displacement sensors.

The relative deviation of the shaft center from the ideal sensor's position introduces detection error due to the curvature effect of the test tool [2]. As is shown in the left part of Fig. 2, the spindle's coordinates are fixed while the sensor's position is changing relatively because of installation error. The installation error includes angle error β and position error l. The function of the detection line in the spindle's coordinates system can be expressed as Eq. 5. And x_0 is defined to describe the combined deviation error by calculating the distance of detection line to shaft center O, and it can be linearized as Eq.10 with an acceptable error (within 5nm when β <2°, $r = 20mm$, $s = 20mm$). It is estimated that $l < 0.1mm$, $\beta < 1°$, in which

case x_0 <0.8mm, according to Eq. 6.

$$y = cot\beta \cdot x + s + r - l \cdot cot\beta \tag{5}$$

$$x_0 = l - \pi(s + r)\beta/180^{\circ} \tag{6}$$

The spindle's coordinates system can be transferred into the standard detection coordinates system by rotating β, as shown in the right part of Fig. 2. By using the Pythagorean Theorem, the centering error E_0 considering both combined installation deviation (x_0), and the deviation caused by loads (d) can be calculated. Since the rotating orbit in load condition varies in an envelope circle, the d in Eq. 7 need to be replaced by $d(\theta)$. Equation 7 is transformed into Eq. 8 by linearization (error within 0.1%, when $|x_0| < 1mm, |d| < 0.1mm$).

$$E_0(d, x_0) = \sqrt{r^2 - (x_0 + d)^2} - \sqrt{r^2 - (x_0)^2} \tag{7}$$

$$E_0(d(\theta), x_0) = d(\theta) \cdot x_0/r - \left(r - \sqrt{r^2 - d(\theta)^2}\right) \tag{8}$$

Regarding the radius of the test tool (r) as a constant value, the specific detection error can be estimated when the value of x_0 and $d(\theta)$ are determined. If the range of these two values is determined, the maximum error can also be estimated. Since the actual installation x_0 is difficult to test, an adjustment procedure is proposed to locate the most suitable position with minimized x_0. The loads introduced deviation of shaft center is explained in Eq. 8, with a dynamic range of $l_{OO'} \pm R(\theta)$. $l_{OO^{prime}}$ can be obtained by the value in the laser displacement sensor in the perpendicular direction. However, $R(\theta)$ is extremely difficult to be measured precisely. Thus it remains as uncertainty error. As such, an adjustment procedure (Fig. 3) is proposed to minimize error caused by installation (x_0) and load-induced error $d(\theta)$.

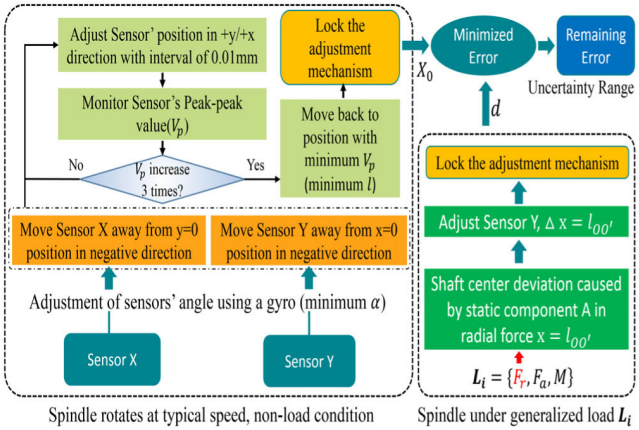

FIGURE 3. Adjustment procedure for minimizing detection error.

III. EVALUATION OF ROTATING PERFORMANCE

The performance evaluation consists of two steps: firstly, the rotating orbit under a specific load condition should be analyzed quantitatively; secondly, the evaluation result of a single load condition is extended to multi-load condition.

A. ROTATING ORBIT IN SPECIFIC LOAD CONDITION

The rotating orbit under unified loads $\boldsymbol{L_i}$ is defined as $\delta(\theta, \boldsymbol{L_i}, n)$. Two displacement sensors in the mutual perpendicular direction (ρ_x and ρ_y) can be used to capture the rotating orbit depicted as Eq. 9.

$$\begin{cases} \rho_x = \delta(\theta, \boldsymbol{L_i}, n)\, cos(30\pi nt + \varphi) + F_r \cdot K_d \\ \rho_y = \delta(\theta, \boldsymbol{L_i}, n)\, sin(30\pi nt + \varphi) \end{cases} \tag{9}$$

where θ is the rotating angle of spindle and K_d represents the dynamic stiffness of spindle, φ is the phase angle.

The blue dots in Fig. 4 are the instant shaft centers, while the depth of their background color indicates the probability density of those dots. It can be seen from Fig. 4 that the static component of the radial force F_r drives the average axial position from unloaded center O to a new center O′. The rotating orbit under the static loads is still circular shape, but the size of the orbit differs from the unloaded rotating orbit. When the dynamic loads exert on the motorized spindle, the rotating orbit will be no longer a determined shape, but dynamically changes within a specific area.

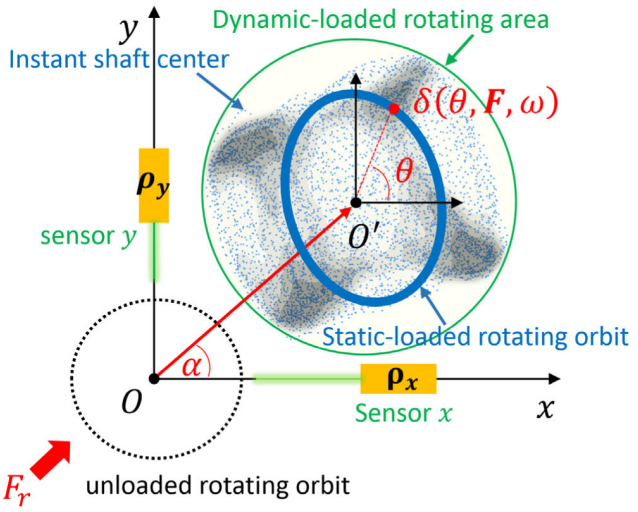

FIGURE 4. Detection of load-dependent rotating orbits.

In order to depict the rotating performance both in loaded and unloaded conditions, the probability enveloping circle that covers most of the instant shaft centers is proposed to quantify the rotating orbit. The shaft center data set is denoted as $M_o\{X, Y\}$, and (x_0, y_0) is one of the shaft centers. Assuming there exists a circle with radius r and center point (a, b), which covers $\gamma\%$ of data set M_o. r_0 is the radius of an existing circle that fully covers all data of M_o.

$$\begin{cases} (x_0 - a)^2 + (y_0 - b)^2 \le r_0 \\ Probability\,(r < r_0) = \gamma\% \\ r_0 \to min \end{cases} \tag{10}$$

The target function can be defined as:

$$r = max(\sqrt{(x_0 - a)^2 + (y_0 - b)^2} \tag{11}$$

Simulated annealing algorithm (SAA) [28] is applied to solve the optimal enveloping radius r and dynamic shaft center $O'(a, b)$. The distance between the unload rotating center and loaded rotating center $l_{OO'}(n, \boldsymbol{L_i})$ is the axis displacement error (ADE) while the minimum radius of envelope circle $R(n, \boldsymbol{L_i})$ represents the rotating error (RE). The sum of these two values can be regarded as

Comprehensive Position Error (CPE) under the load condition noted as $P(n, \boldsymbol{L_i})$.

$$P(n, \boldsymbol{L_i}) = l_{OO'}(n, \boldsymbol{L_i}) + R(n, \boldsymbol{L_i}) \tag{12}$$

B. MULTI-CONDITIONS PERFORMANCE EVALUATION

A novel idea of Multi-Zones Error Map (MZE Map) is designed to exhibit the radial rotating error under different loads conditions in a visual way. In the MZE Map, x, y, z axis are defined as the speed axis, load axis, and performance axis, respectively. A series of tests with respect to the rotating performance need to be conducted, and their results are arranged in the following five zones: static deformation test zone (Zone-I), bearings clearance test zone (Zone-II), dynamic deformation test zone (Zone-III), speed-dependent rotating test zone (Zone-IV), and typical load condition test zone (Zone-V).

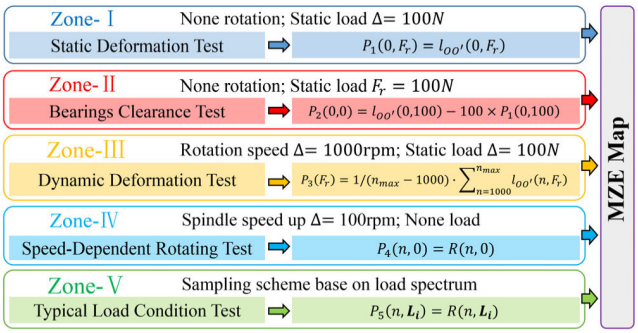

FIGURE 5. Flowchart of establishing the MZE Map.

There are five procedures to establish the MZE Map, as summarized in Fig. 5. Firstly, the static deformation under radial force F_r is calculated by $l_{OO'}$. At least three different angle positions of the spindle should be tested for an average result. Secondly, the bearings clearance test is introduced because this clearance condition affects both the stiffness and rotating precision of a spindle. A simplified test method is substituting the displacement calculated by stiffness value from the actual displacement:

$$P_2(0, 0) = l_{OO'}(0, 100) - 100 \times P_1(0, 100) \tag{13}$$

Thirdly, the dynamic deformation test is carried out to inspect the average radial deformation error of the spindle under radial loads. Since there is little difference in dynamic deformation of different rotation speed, an average deformation of different speeds (from 1000rpm to n_{max}) is used to calculate $P_3(F_r)$. Fourthly, the speed-dependent rotation performance (P_4) is tested by collecting the unloaded rotation radius $R(n, 0)$ with a speed interval of 100 r/min.

Motorized spindle operates under countless speed and load combinations, but several typical load conditions may be summarized by statistical method from the field data. This typical load scheme is called a load spectrum in engineer for the guidance of spindle design and experiment [29], [30]. Because it is impossible to test all the load conditions in Zone-V, a typical load area is defined considering the range of speed in x axis, and the maximum and minimum load range in y axis (Fig. 6). The most typical load conditions are marked in red spots in the typical load area, which stands for the most frequently appeared speed and load combinations. Therefore, in the fifth step, the typical load condition test is applied by selecting some representative load conditions, and the rotating error under each typical load conditions is donated as $P_5(n, \boldsymbol{L_i})$. Besides, the rotating error under the dominant loads (the static component of $\boldsymbol{L_i}$) is tested as a reference index and rotating performance.

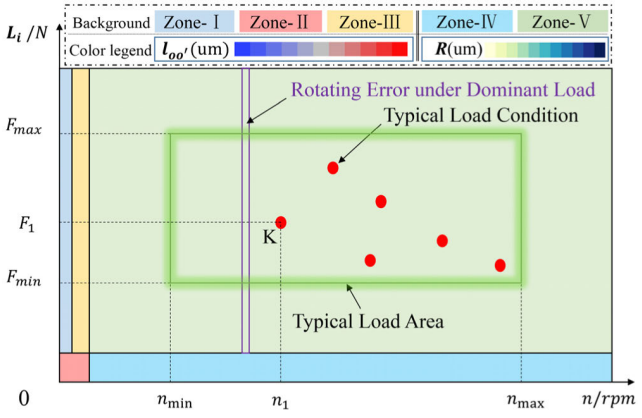

FIGURE 6. Design scheme of proposed MZR Map.

Finally, the MZE Map can be produced by integrating the five test results into different zones according to their test properties, as shown in Fig. 6. The test results are represented in axis displacement error ($l_{OO'}$) in Zone-I, Zone-II, and Zone-III. Nevertheless, in Zone-IV and Zone-V, since the rotating error is relevant with the speed-load combination, the rotating error (R) is used as the evaluation value in these two zones.

The MZE Map is a visual tool for expressing both the spindle's ADE and RE. Each test result under a specific speed-load combination (for example, in point K, speed = $\boldsymbol{n_1}$, dominant loads $\boldsymbol{L_i} = F_1$) can be marked in a colored block according to the color legend of MZE Map. The MZE Map evaluates the performance of rotating movement in different speed-load combinations, which guides the selection of most appropriate operating parameters. In real operation, $P_3(A)$ can be compensated by the Number Control system, while $R(n, \boldsymbol{L_i})$ is difficult to be eliminated due to its uncertainty. The Comprehensive Position Error (CPE) in the rotating movement can be summed as the combination of two

parts in the MZE Map, which serves as the overall index for evaluating the rotating performance of the motorized spindle.

$$P(n, \boldsymbol{L}_i) = P_3(A) + R(n, \boldsymbol{L}_i) \tag{14}$$

IV. EXPERIMENT

In this section, a load simulation test platform applying the proposed unified load function is established, after which the measurement error is discussed. Several loading contrast tests are performed to demonstrate the difference in rotating performance under various load conditions. An example of performance evaluation based on the proposed MZE Map is conducted with a vivid result of deformation error and rotating error of tested spindle under different operation conditions.

A. LOAD SIMULATION TEST PLATFORM

A load simulation test platform provides the experiment foundation for the proposed evaluation method. The cutting force is simulated using an electronic-hydraulic servo actuator with closed-loop control software, while the torque is generated by a dynamometer. A cylindrical test tool is installed in the motorized spindle in the same way as the real cutting tool, transferring the workload from the loading device to the motorized spindle. As displayed in Fig. 7, the radial force is exerted directly on the force convert unit while the axial force is transferred to the force convert unit through a lever mechanism. There is a pair of bearings inside the force convert unit, which can transmit radial and axial force from the shell to the test tool. The other end of test tool is connected to a dynamometer through a diaphragm coupling, which transfers the torque loads to the motorized spindle.

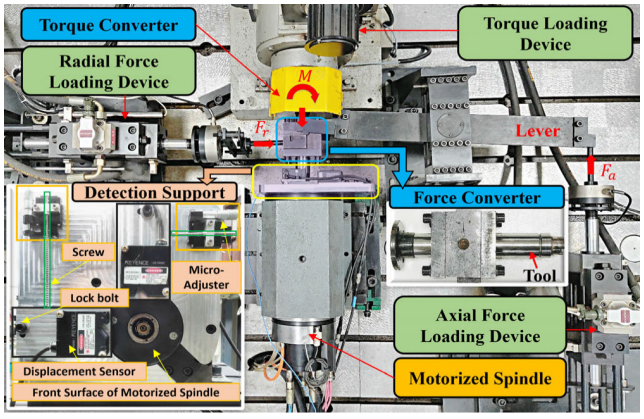

FIGURE 7. Load simulation test platform of the motorized spindle.

A pair of mutually perpendicular laser displacement sensors is installed on the sensor support to capture the rotating orbit at the 30mm axial position of the test tool. The aluminum-made sensor support is strongly locked on the front surface of the motorized spindle via the bolt connection. The position of the laser can be adjusted manually with the micro-screw mechanism of a 2um solution. Some of the critical indexes on the platform are listed in Table 1.

TABLE 1. System parameters of test platform.

Item	Type	Description
Motorized spindle	ZYS-160XDS30Q Machining Center's	T_{max}=9.5N.m, Power: 22kw n_{max}=22000rpm, HSK E40
Loading device	Force	F_{max}=10kN, f_{max}=60Hz
	Torque	$T_{max} = 20Nm$, Power: 22kw
Data Acquisition	DAQ card	NI cDAQ system, NI-9234
	Displacement sensor	Keyence-LK-H050, 0.025um

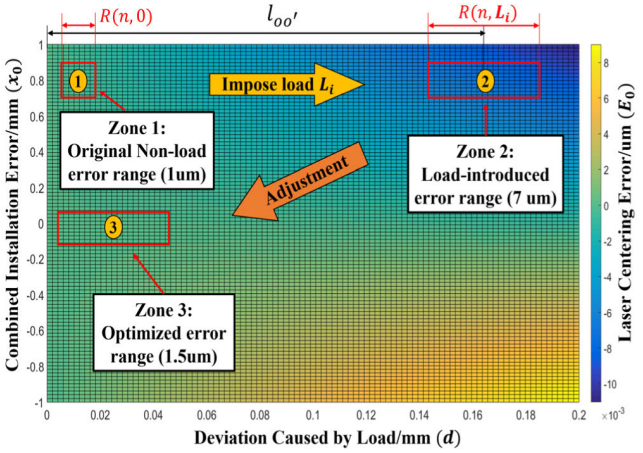

FIGURE 8. Calculation result of centering error.

B. MEASUREMENT ERROR ANALYSIS

The calculation results of centering error (E_0) introduced by combined installation error (x_0) and loaded error (d) are calculated in Fig. 8. Assuming that the initial installation position x_0 is 0.8mm ($l = 0.1mm$, $\beta = 1°$ cases in existing test platform), the error in the unloaded condition is less than 1um. When $F_{rmax} = 1800$N, the error area shifts to zone 2, with a load-induced error of 7um. After adjusting the displacement sensor's position to zone 3, the E_0 can be reduced to 1.5um.

The maximum vibration displacement of sensor support (V_x, V_y) is tested to be 0.6um, which can be alleviated by the MAF filter [30]. A modal test on the sensor support was conducted to confirm that resonant frequencies in all directions were higher than the tested rotating frequency (4000rpm/66Hz).

Adding the error in the loading system, the overall error in the radial force loading direction E_x, and the overall error perpendicular to the radial loading direction E_y can be expressed as:

$$E_x = E_0(0.1, R(n,0)) + V_x + F_r \cdot (1 - cos\alpha)/k \tag{15}$$

$$E_y = E_0(0.1, R(n, \boldsymbol{L_i})) + V_y + F_r \cdot sin\alpha/k \tag{16}$$

The installing deviation angle α in the loading system can be adjusted within 0.5°. x_0 is controlled within 0.1mm using the micro-adjuster. The deviation under the maximum radial force ($F_{rmax} = 1800$N) is tested to be 0.138 mm. According to the simulation result in Fig. 8 and the above formulas, it can be estimated that $E_x < 1.6$um, $E_y < 3.3$um. Since

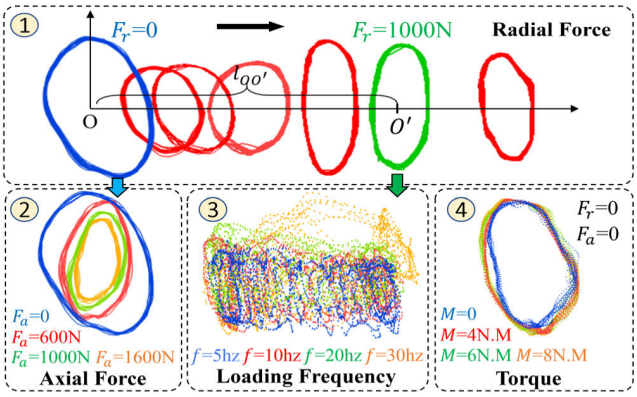

FIGURE 9. Effect of different loads on the shaft's rotating orbit.

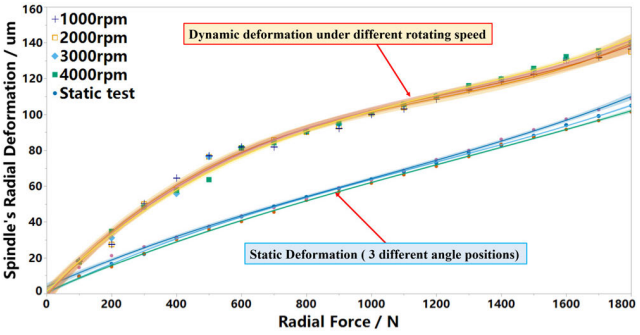

FIGURE 10. Axis displacement error of tested motorized spindle.

the evaluation result of the envelope circle is mainly dependent on the load-introduced direction (radial force direction), the error E_y has little contribution to the ultimate results.

C. TEST RESULTS

Four comparison tests of spindle's rotating orbit under different radial force, axial force, force-frequency (f), and torque are presented in Fig. 9 (in a typical rotation speed of 3000rpm). It can be observed from each test that: (1) as the radial force increases, the axis displacement error $l_{OO'}$ becomes more significant in force direction while the radius of rotation error R first increases and then decreases, and the rotating radius is rather large due to the bearings clearance when $F_r = 0$; (2) as the axial force increases, the rotation error of the spindle is reduced; (3) the rotating orbit's become chaos, and its movement area becomes more significant as loading frequency increases ($A = 1000N$, $\varepsilon = 200N$); (4) rotating orbit has little relationship with torque.

The experiment for establishing the proposed MZE Map is performed following the flowchart (Fig. 5). The radial deformation of the spindle under different radial force is tested (Fig. 10). The result confirms that the static deformation is almost linear, but the dynamic deformation is nonlinear with the radial force. The rotating speed hardly affects dynamic stiffness, which means the average dynamic stiffness is capable of estimating dynamic deformation in any rotating speed. To sum up, the average value of static and

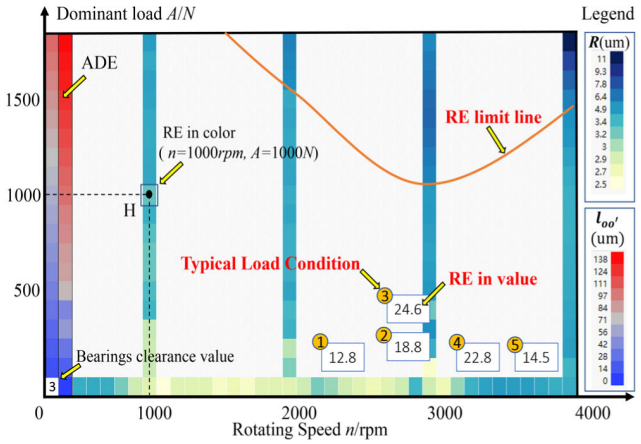

FIGURE 11. MZE Map of tested motorized spindle.

TABLE 2. Modal test result for sensor support.

Direction	First Model	Second Model
X-direction	351Hz	604 Hz
Y-direction	354 Hz	527 Hz
Z-direction	906 Hz	1425 Hz

dynamic deformation of spindle under different loads can be calculated as $P_1(F_r)$ and $P_3(F_r)$, and they can be transferred into colored indicators in the left two columns of MZE Map (Zone-I and Zone-III in Fig. 11). The bearing clearance is tested to be 3um and is marked near the original point of the MZE Map (Zone-II in Fig. 11).

The speed-dependent rotating error is tested with a speed interval of 100rpm (range from 500rpm to 4000rpm), and the results are presented in the bottom row with colored indicators in the MZE Map (Zone-IV in Fig. 11). The speed-dependent rotating error first decreases and then increases with rotating speed. In 2300rpm and 2800rpm, the rotating error is much larger than the nearby speed. It shows that better rotating performance can be achieved when this less-desired condition is avoided according to the color indicator in the MZE Map.

The typical parameters in milling processes are collected in a machining factory [31] to compile a corresponding load spectrum, and it is further adjusted into the unified load function according to Eq. 4 (as shown in Table 3). In the milling process, the radial force is defined as the dominant loads, and the noise function $\sigma(t)$ is considered as zero for simplification.

Due to the diversity of parameters in $\boldsymbol{L_i}$, it takes several MZE Maps to describe mill, drilling, and boring process individually. Take milling operation, for example, and static radial force is exerted on the spindle at 1000rpm, 2000rpm, 3000rpm, and 4000rpm. As shown in Fig. 11, the rotating error alters with the loads in a nonlinear way, and a RE limit line is drawn to separate the speed-load conditions where rotating error exceeds alarm value (6 um, for example). When the dynamic cutting force is exerted on the motorized spindle

TABLE 3. Load spectrum in milling for typical loads test.

Condition No.	1	2	3	4	5
n: Rotating speed (r/min)	2500	3000	3000	3500	4000
A: Mean of F_r (N)	52	228	396	48	161
ε: Amplitude of F_r (N)	334	494	803	171	294
k_1: Radial force factor	1	1	1	1	1
k_2: Axial force factor	0.1	0.62	0.49	0.29	0.65
k_3: Torque factor (m)	0.04	0.007	0.005	0.015	0.009
R: Tested Rotating Error	12.8	18.8	24.6	22.8	14.5

according to the five typical load conditions according to Table 3, the result of dynamic rotating performance is marked with RE in value in the MZE Map, which can distinguish the rotating performance of the tested spindle under several speed-load conditions.

V. CONCLUSION

This paper extends the measurement and evaluation dimension of the conventional speed-dependent performance by introducing a load-dependent performance methodology. In the beginning, a unified load function is set up as the basic pattern for loading tests. Then, the rotating performance test is performed on a load simulating system with rotating orbit acquisition ability. Adjustment of the laser displacement sensors needs to be performed to reduce the evaluation error. The overall evaluation error in the proposed envelope circle is less than 1.6um.

It has been demonstrated from several contrast tests that it is of great value to fully evaluate the load-dependent rotating performance because the rotating orbit varies a lot under different kinds of loads: (1) the radial loads not only affect the rotating error but also changes the shaft's average position, and the increase of loading frequency complicates rotating orbit; (2) there is a negative correlation between the axial force and the rotating error, and the axial force will not produce axis displacement error; (3) the cutting torque has little influence on the radial rotating orbit.

In order to comprehensively present various test results related to load-dependent rotating performance, this paper introduces a novel test scheme of MZE Map. It provides a vivid experimental basis for evaluating the rotating performance, considering different speeds and loads. It also serves as a new approach for the performance test for motorized spindles. The evaluation results not only include existing performance indexes such as rotary accuracy and stiffness but also exhibit a wide range of information concerning rotating performance and quality under typical load conditions. In fact, the evaluation results can hardly predict the actual machining accuracy of the tested motorized spindle, due to the diversity in the size, material, and dynamic characteristics of cutting tools in the machining process. Nevertheless, the outcome of the MZE Map is a machining-free calibration method of locating less desirable conditions in rotating, selecting the favorable workload combinations with excellent rotating performance.

REFERENCES

[1] E. Abele, Y. Altintas, and C. Brecher, "Machine tool spindle units," *CIRP Ann.*, vol. 59, no. 2, pp. 781–802, 2010, doi: 10.1016/j.cirp.2010.05.002.

[2] K. P. Anandan, A. S. Tulsian, A. Donmez, and O. B. Ozdoganlar, "A Technique for measuring radial error motions of ultra-high-speed miniature spindles used for micromachining," *Precis. Eng.*, vol. 36, no. 1, pp. 104–120, Jan. 2012, doi: 10.1016/j.precisioneng.2011.07.014.

[3] T. L. Schmitz, J. Couey, E. Marsh, N. Mauntler, and D. Hughes, "Runout effects in milling: Surface finish, surface location error, and stability," *Int. J. Mach. Tools Manuf.*, vol. 47, no. 5, pp. 841–851, Apr. 2007, doi: 10.1016/j.ijmachtools.2006.06.014.

[4] H. Cao, X. Zhang, and X. Chen, "The concept and progress of intelligent spindles: A review," *Int. J. Mach. Tools Manuf.*, vol. 112, pp. 21–52, Jan. 2017, doi: 10.1016/j.ijmachtools.2016.10.005.

[5] W. Chen, Z. Yang, C. Chen, and F. Chen, "Health condition evaluation method for motorized spindle based on rotation error and vibration," in *Proc. Annu. Rel. Maintainability Symp. (RAMS)*, Reno, NV, USA, Jan. 2018, pp. 1–7, doi: 10.1109/RAM.2018.8463038.

[6] P. Ma, C. Zhao, C. Gong, X. Niu, and X. Lu, "Rotation error measurement technology and experimentation research of high-precision hydrostatic spindle," *Int. J. Adv. Manuf. Technol.*, vol. 73, nos. 9–12, pp. 1313–1320, 2014, doi: 10.1007/s00170-014-5905-5.

[7] H. Cao, B. Li, and Z. He, "Chatter stability of milling with speed-varying dynamics of spindles," *Int. J. Mach. Tools Manuf.*, vol. 52, no. 1, pp. 50–58, 2012, doi: 10.1016/j.ijmachtools.2011.09.004.

[8] *Test Code for Machine Tools—Part 7: Geometric Accuracy of Axes of Rotation*, Standard ISO 230-7:2015, 2006.

[9] K. P. Anandan and O. B. Ozdoganlar, "Analysis of error motions of ultra-high-speed (UHS) micromachining spindles," *Int. J. Mach. Tools Manuf.*, vol. 70, pp. 1–14, Jul. 2013, doi: 10.1016/j.ijmachtools.2013.02.005.

[10] S. Nahata, R. Onler, E. Korkmaz, O. B. Ozdoganlar, and S. Shekhar, "Radial throw in micromachining: Measurement and analysis," *Precis. Eng.*, vol. 54, pp. 21–32, Oct. 2018, doi: 10.1016/j.precisioneng.2018.04.005.

[11] F. Chaari, W. Bartelmus, R. Zimroz, T. Fakhfakh, and M. Haddar, "Gearbox vibration signal amplitude and frequency modulation," *Shock Vib.*, vol. 19, no. 4, pp. 635–652, 2012, doi: 10.3233/SAV-2011-0656.

[12] B. Bediz, B. A. Gozen, E. Korkmaz, and O. B. Ozdoganlar, "Dynamics of ultra-high-speed (UHS) spindles used for micromachining," *Int. J. Mach. Tools Manuf.*, vol. 87, pp. 27–38, Dec. 2014, doi: 10.1016/j.ijmachtools.2014.07.007.

[13] M. Ritou, C. Rabréau, B. Furet, D. Dumur, and S. Le Loch, "Influence of spindle condition on the dynamic behavior," *CIRP Ann.*, vol. 67, no. 1, pp. 419–422, 2018, doi: 10.1016/j.cirp.2018.03.007.

[14] Y. Chen, X. Liang, and M. J. Zuo, "Time series modeling of vibration signals from a gearbox under varying speed and load condition," in *Proc. IEEE Int. Conf. Prognostics Health Manage.*, Seattle, WA, USA, Jun. 2018, pp. 1–7, doi: 10.1109/ICPHM.2018.8449003.

[15] S. Ibaraki, Y. Nagai, Y. Sakai, S. Morimoto, Y. Miyazaki, and S. Tsujimoto, "A pyramid-shaped machining test to identify rotary axis error motions on five-axis machine tools: Software development and a case study," *Int. J. Adv. Manuf. Technol.*, vol. 94, nos. 1–4, pp. 227–237, Jan. 2018, doi: 10.1007/s00170-017-0906-9.

[16] D. Tlalolini, M. Ritou, C. Rabréau, S. Le Loch, and B. Furet, "Modeling and characterization of an electromagnetic system for the estimation of Frequency Response Function of spindle," *Mech. Syst. Signal Process.*, vol. 104, pp. 294–304, May 2018, doi: 10.1016/j.ymssp.2017.11.003.

[17] C. Yue, H. Gao, X. Liu, S. Y. Liang, and L. Wang, "A review of chatter vibration research in milling," *Chin. J. Aeronaut.*, vol. 32, no. 2, pp. 215–242, Feb. 2019, doi: 10.1016/j.cja.2018.11.007.

[18] T. Shimoda and H. Fujimoto, "Adaptive spindle-speed selection for chatter avoidance to achieve high-precision NC machining based on semi-discretization method," in *Proc. 43rd Annu. Conf. IEEE Ind. Electron. Soc. (IECON)*, Beijing, China, Oct./Nov. 2017, pp. 6709–6714, doi: 10.1109/IECON.2017.8217172.

[19] G. Mirzaeva, K. I. Saad, and M. G. Jahromi, "Comprehensive diagnostics of induction motor faults based on measurement of space and time dependencies of air gap flux," *IEEE Trans. Ind. Appl.*, vol. 53, no. 3, pp. 2657–2666, May/Jun. 2017, doi: 10.1109/ TIA.2016.2628718.

[20] M. Kaymakci, Z. M. Kilic, and Y. Altintas, "Unified cutting force model for turning, boring, drilling and milling operations," *Int. J. Mach. Tools Manuf.*, vols. 54–55, pp. 34–45, Mar./Apr. 2012, doi: 10.1016/j.ijmachtools.2011.12.008.

[21] Z. M. Kilic and Y. Altintas, "Generalized mechanics and dynamics of metal cutting operations for unified simulations," *Int. J. Mach. Tools Manuf.*, vol. 104, pp. 1–13, May 2016, doi: 10.1016/j.ijmachtools.2016.01.006.
[22] C. Eksioglu, Z. M. Kilic, and Y. Altintas, "Discrete-time prediction of chatter stability, cutting forces, and surface location errors in flexible milling systems," *J. Manuf. Sci. Eng.*, vol. 134, no. 6, Dec. 2012, Art. no. 061006, doi: 10.1115/1.4007622.
[23] A. Lamikiz, L. N. L. de Lacalle, J. A. Sánchez, and M. A. Salgado, "Cutting force estimation in sculptured surface milling," *Int. J. Mach. Tools Manuf.*, vol. 44, no. 14, pp. 1511–1526, Nov. 2004, doi: 10.1016/j.ijmachtools.2004.05.004.
[24] J. C. Roukema and Y. Altintas, "Generalized modeling of drilling vibrations. Part I: Time domain model of drilling kinematics, dynamics and hole formation," *Int. J. Mach. Tools Manuf.*, vol. 47, no. 9, 2007, pp. 1455–1473, doi: 10.1016/j.ijmachtools.2006.10.005.
[25] M.-B. Lazar and P. Xirouchakis, "Mechanical load distribution along the main cutting edges in drilling," *J. Mater. Process. Technol.*, vol. 213, no. 2, pp. 245–260, Feb. 2013, doi: 10.1016/j.jmatprotec.2012.09.020.
[26] I. Lazoglu, F. Atabey, and Y. Altintas, "Dynamics of boring processes: Part III-time domain modeling," *Int. J. Mach. Tools Manuf.*, vol. 42, no. 14, pp. 1567–1576, Nov. 2002, doi: 10.1016/S0890-6955(02)00067-6.
[27] E. Budak, Y. Altintas, and E. J. A. Armarego, "Prediction of milling force coefficients from orthogonal cutting data," *J. Manuf. Sci. Eng.*, vol. 118, no. 2, pp. 216–224, 1996, doi: 10.1115/1.2831014.
[28] S. Bandyopadhyay, S. Saha, U. Maulik, and K. Deb, "A simulated annealing-based multiobjective optimization algorithm: AMOSA," *IEEE Trans. Evol. Comput.*, vol. 12, no. 3, pp. 269–283, Jun. 2008, doi: 10.1109/TEVC.2007.900837.
[29] G. Li, J. He, K. Wu, C. Zhou, and S. Wang, "Compilation of load spectrum of machining center spindle and application in fatigue life prediction," *J. Mech. Sci. Technol.*, vol. 33, no. 4, pp. 1603–1613, Apr. 2019, doi: 10.1007/s12206-019-0312-3.
[30] S. Golestan, M. Ramezani, J. M. Guerrero, F. D. Freijedo, and M. Monfared, "Moving average filter based phase-locked loops: Performance analysis and design guidelines," *IEEE Trans. Power Electron.*, vol. 29, no. 6, pp. 2750–2763, Jun. 2014, doi: 10.1109/TPEL.2013.2273461.
[31] D. Zhu, C. Chen, X. Du, G. Li, X. Li, and Z. Yang, "Compilation of program-loading spectrum for milling of a motorized spindle based on cutting force model," *J. Brazilian Soc. Mech. Sci. Eng.*, vol. 41, p. 187, Apr. 2019, doi: 10.1007/s40430-019-1686-y.

WEIZHENG CHEN was born in Fujian, China, in 1992. He received the B.S. degree in mechatronics engineering from the Changchun University of Science and Technology, in 2015, and the master's degree from the Key Laboratory of CNC Equipment Reliability of Education Ministry, Jilin University, where he is currently pursuing the Ph.D. degree in mechanical engineering. His main research interests are reliability engineering, prognostic, and health management of CNC equipment. He specializes in the developing and programming of condition monitoring systems. Besides, the data mining and feature analysis under a complicated situation are also within his research domain.

ZHAOJUN YANG received the Ph.D. degree in mechanical engineering from the Jilin University of Technology, in 1995. He is currently a Professor with the School of Mechanical and Aerospace Engineering, Jilin University. He is also the Director of the Key Laboratory of CNC Equipment Reliability of Education Ministry. He is also granted as the Changbai Mountain Scholars Distinguished Professor and enjoys special government allowances from the State Council of China. He has been in charge of over 30 projects involving national science and technology major projects and published over 100 articles of reliability field. His main research interests are reliability theory and technology of computer numerical control equipment.

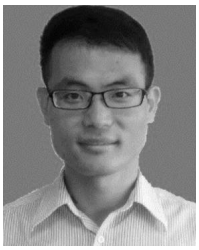

CHUANHAI CHEN received the B.S. degree in mechanical manufacturing and automation from Southwest Jiaotong University, in 2008, and the Ph.D. degree in mechanical engineering from Jilin University, in 2013. He is currently an Associate Professor with the School of Mechanical and Aerospace Engineering, Jilin University. He has undertaken and participated in over ten projects involving national science and technology major projects and published over 20 articles in related field. His main research interests are on load spectrum analysis of CNC machine tools, reliability accelerated test technology, and reliability modeling and evaluation technology of intelligent manufacturing equipment.

WEI LUO was born in 1986. She received the master's degree in mechanical engineering, in 2011. She is currently pursuing the Ph.D. degree with Jilin University, China. She worked with the Changchun Equipment and Technology Research Institute. She is also an Associate Professor with the School of Mechanical and Aerospace Engineering, Jilin University. Her research interests include CNC equipment and its functional parts reliability theory, application technology research, and structure design and optimization.